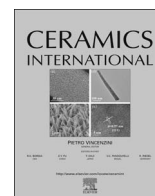




Contents lists available at ScienceDirect

Ceramics International

journal homepage: www.elsevier.com/locate/ceramint

Effect of Zr substitution on structural, magnetic, and optical properties of $\text{Bi}_{0.9}\text{Dy}_{0.1}\text{Fe}_{1-x}\text{Zr}_x\text{O}_3$ multiferroic ceramics prepared by rapid liquid phase sintering method

Prakash Chandra Sati^{a,*}, Manoj Kumar^b, Manisha Arora^c, Monika Tomar^d, Vinay Gupta^a

^a Department of Physics and Astrophysics, University of Delhi, Delhi 110007, India

^b Department of Physics and Materials Science and Engineering, Jaypee Institute of Information Technology, Noida 201301, India

^c Department of Applied Science, Krishna Engineering College, Ghaziabad 201006, India

^d Physics Department, Miranda House, University of Delhi, Delhi 110007, India

ARTICLE INFO

Keywords:

B. X-ray methods
B. Electron microscopy
C. Magnetic properties
C. Optical properties

ABSTRACT

Zr substituted $\text{Bi}_{0.9}\text{Dy}_{0.1}\text{Fe}_{1-x}\text{Zr}_x\text{O}_3$ ($x=0.03, 0.06$ and 0.10) multiferroic ceramics were synthesized by rapid liquid phase sintering technique to improve its multiferroic properties. Rietveld structural refinement of XRD patterns and Raman spectra revealed a partial structural phase transition from rhombohedral ($R3c$) to biphasic structure ($R3c+P4mm$) on codoping. The substitution of larger ionic radii and higher valence Zr^{4+} ions at Fe-site leads to decrease in the grain size as a result of charge compensation at Fe site. The weak ferromagnetic behavior were observed in all samples along with maximum M_s value of 0.159 emu/g for $x=0.03$ concentration, which is also endorsed by second order Raman modes. The distortion in FeO_6 octahedra due to Zr substitution leads to splitting of electronic bands of 3.2 eV into multiplets, which in turn reduced the optical band gap value in the range of $2.06\text{--}2.10 \text{ eV}$ for all samples.

1. Introduction

Multiferroic materials simultaneously possess two or more ferroic properties like ferroelectricity, ferromagnetism and ferroelasticity in the single phase. BiFeO_3 (BFO) is most studied material due to its high ferroelectric transition temperature ($T_c=1103 \text{ K}$) and ferromagnetic transition temperature ($T_N=643 \text{ K}$). BFO possesses distorted rhombohedral structure with $R3c$ space group. The magnetic structure of BFO is antiferromagnetic along with G-type spiral spin structure with a period of 62 nm [1]. The inhomogeneous spiral spin structure of Bismuth ferrite leads to cancellation of the macroscopic magnetization which prohibits the linear magnetoelectric effect from being observed in bulk BFO ceramics. To remove the problems associated with BFO, many attempts have been made recently (i) substitution at Bi-site by Dy^{3+} , Pr^{4+} , Ho^{3+} ions [2–4] (ii) substitution at Fe-site by Mn^{3+} , Zr^{4+} , Ti^{4+} , Nb^{5+} ions [5–8] (iii) co-substitution at Bi/Fe-site by $\text{Pr}^{3+}/\text{Zr}^{4+}$, $\text{La}^{3+}/\text{Zr}^{4+}$, $\text{Ca}^{2+}/\text{Ti}^{4+}$, $\text{Sr}^{3+}/\text{Ti}^{4+}$, $\text{Pr}^{3+}/\text{Cr}^{3+}$ ions [9–13]. Among the various kinds of methods to improve the multiferroic properties, doping at A and B sites is quite effective and it is much helpful to further enhance the multiferroic properties of BFO in bulk ceramics, nanoparticles and thin film [11,14,15]. Because the ferroelectricity and magnetism in BFO come from the lone pair electrons of Bi^{3+} ions and

partially filled d orbital of Fe^{3+} ions, respectively. Among various kinds of doping reported at Fe-site, Zr^{4+} substitution is found particularly attractive. There are several reports on independently Dy^{3+} and Zr^{4+} substituted BFO ceramics but none about co-substitution of Dy^{3+} and Zr^{4+} simultaneously. Therefore, in the present work, $\text{Bi}_{0.9}\text{Dy}_{0.1}\text{Fe}_{1-x}\text{Zr}_x\text{O}_3$ multiferroic are synthesized using rapid liquid phase sintering technique and studied their details structural, morphological, magnetic and optical properties.

2. Experimental details

Zr substituted $\text{Bi}_{0.9}\text{Dy}_{0.1}\text{Fe}_{1-x}\text{Zr}_x\text{O}_3$ with $x=0.03, 0.06$ and 0.10 has been synthesized via rapid liquid phase sintering method. High purity powders of Bi_2O_3 , Dy_2O_3 , Fe_2O_3 , and ZrO_2 were used as starting chemical reagents. These chemicals were carefully weighed in stoichiometric ratio, mixed and ground in an acetone medium for 10 h to get homogeneously mixed fine powder. Now, the mixed powder is then pressed into pellets of thickness 1 mm and diameter 10 mm and heat treated at $900 \text{ }^\circ\text{C}$ for very short time duration ($\sim 15 \text{ min}$) in tubular furnace. The phase purity and crystal structure of samples were determined by X-ray diffraction (Bruker D8 Advance) with $\text{CuK}\alpha$ radiation. The X-ray diffraction (XRD) data were analysed by using

* Corresponding author.

E-mail address: satimt8311956@gmail.com (P.C. Sati).

<http://dx.doi.org/10.1016/j.ceramint.2016.12.141>

Received 18 August 2016; Received in revised form 30 December 2016; Accepted 30 December 2016
0272-8842/ © 2016 Published by Elsevier Ltd.

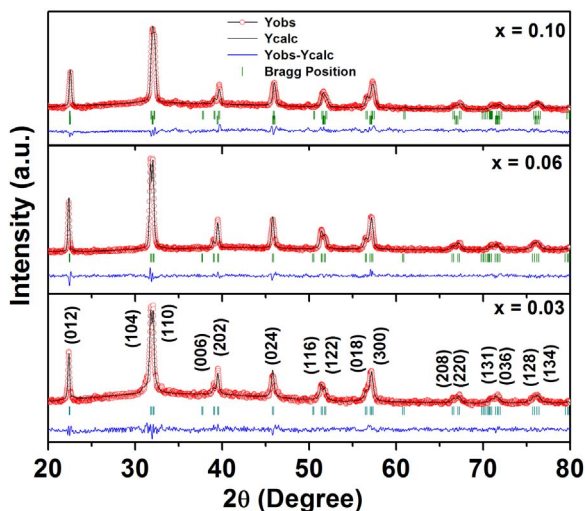


Fig. 1. Rietveld refinement of the XRD patterns of $\text{Bi}_{0.9}\text{Dy}_{0.1}\text{Fe}_{1-x}\text{Zr}_x\text{O}_3$ ceramics with $x=0.03, 0.06$ and 0.10 .

FullProf programme to get detailed structural parameters of the samples. Raman spectra were recorded by Renishaw Raman spectrophotometer using monochromatic radiation emitted by Ar^+ ion laser (wavelength ~ 514.5 nm) operating at 50 mW power. The surface morphology of ceramics was determined using Field emission scanning electron microscope (FESEM). Magnetic properties were measured by superconducting quantum interference device (SQUID). Ultraviolet-visible diffuse reflectance spectra (UV-vis DRS) of the samples were measured by Ocean optics UV-Visible 4000.

3. Results and discussion

Fig. 1 shows Rietveld refined XRD diffraction patterns of $\text{Bi}_{0.9}\text{Dy}_{0.1}\text{Fe}_{1-x}\text{Zr}_x\text{O}_3$ ceramics sintered at 900°C . With increasing Zr concentration, XRD pattern is observed to shift slightly towards lower angle for $x=0.06$ which shifts towards higher angle for $x=0.10$ sample. This shift in XRD pattern indicates that dopants get substituted in BFO. Moreover, a closer examination of the XRD patterns revealed about the tendency of merging of diffraction peaks (104) and (110) into a single broadened peak in the range of $31.5\text{--}32.5^\circ$ for $x=0.10$ sample as shown in Fig. 2. Such a behavior indicates a partial structural transformation from rhombohedral structure (with $R3c$ space group) to tetragonal structure (with $P4mm$ space group) for sample $x=0.10$.

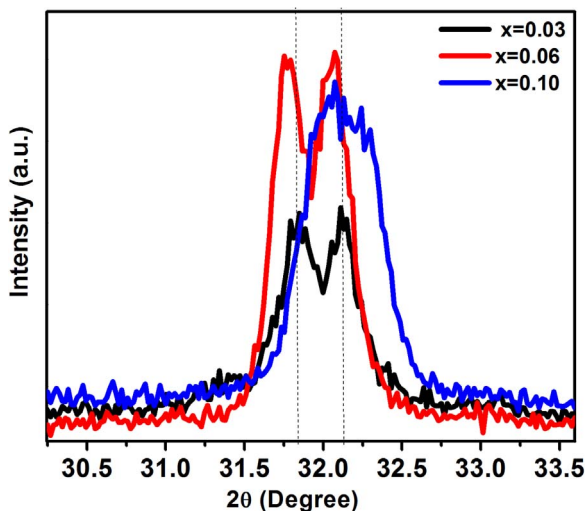


Fig. 2. Magnified XRD pattern around $2\theta=32^\circ$ for $\text{Bi}_{0.9}\text{Dy}_{0.1}\text{Fe}_{1-x}\text{Zr}_x\text{O}_3$ ceramics with $x=0.03, 0.06$ and 0.10 .

Thus, samples with Zr concentration from $x=0.03$ to 0.06 maintained its parent rhombohedral structure, whereas sample with $x=0.10$ is observed to have both $R3c$ (67.76%) and $P4mm$ (32.24%) space group, indicating the two phase coexistence. Similar phase transition has been observed in Er doped BFO ceramics [16] and Ba-Mn co-doped BFO ceramics [17].

The detailed structural analysis of codoped samples has been performed by Rietveld refinement using “FullProf” software. From Rietveld refinement, we have measured variation of lattice constants (a , b and c), lattice volume (V), bond length (Bi/Dy-O and Fe/Zr-O), bond angle (Fe-O-Fe) and positional coordinates (x , y , z) with Zr doping. The Rietveld analysis of the samples is performed by using rhombohedral structure of $R3c$ with wyckoff positions of Bi/Dy at 6a, Fe/Zr at 6a and O at 18b and $P4mm$ space group with wyckoff positions of Bi/Dy at 1a, Fe/Zr at 1b, O_1 at 1b and O_2 at 2c. The Bragg peaks are modelled according to Pseudo-Voigt function and the background was estimated according to linear interpolation between selected background points. The lattice parameters, profile parameters, background parameters, isotropic thermal parameters and atomic positional parameter are refined during Rietveld refinement. After the final cycle of refinement, good matching between observed and calculated XRD patterns has been observed with proper Bragg positions as shown in Fig. 1. The lattice constants (a , b and c), lattice volume (V), bond lengths (Bi/Dy-O, Fe/Zr-O), bond angles (Fe-O-Fe, Bi-O-Bi, Bi-O-Fe), atomic positions of Bi/Dy, Fe/Zr and O and value of R-factors (R_p , R_{wp} , R_{Bragg} and R_F) are listed in Table 1 and Table 2. The average crystallite size is calculated from Debye Scherer formula: $d = K\lambda/\beta\cos\theta$, where d denotes the crystallite size, β is the half-width of the diffraction peak (012), θ stands for the angle corresponding to the position of the Bragg peak and λ is the used wavelength. The value of the constant K in the Scherrer's equation was assumed $K=0.9$. The average crystallite size calculated from Debye Scherer's formula was found to be 41 nm, 39 nm and 25 nm for $x=0.03\text{--}0.10$ samples respectively. In general, crystallite size decreases with increase of substituents due to size mismatching of host and substituted cations which in turn leads to the disorder in the local structure of the samples. Consequently, the induced chemical pressure inside lattice leads to decreases in nucleation rate resulting in decrements in crystallite size.

The FESEM images of codoped samples were shown in Fig. 3. All samples have dense and non-uniform morphology with few pores. The substitution of Dy^{3+} ions at Bi-site help to reduce the volatilization of Bismuth atoms because of higher bond strength of Dy-O bond (611 ± 42 kJ/mol) than that of Bi-O (343 ± 6 kJ/mol). Furthermore, the substitution of non magnetic Zr^{4+} plays an important role of donor ions in BFO because of higher valance than Fe^{3+} ions and suppress oxygen vacancies as a result of charge compensation. Moreover, the addition of Zr to BFO leads to reduction of oxygen vacancy concentration because of stronger Zr-O bond in comparison of Fe-O bond as well as the presence of any Fe^{2+} ions at Fe-site will also be compensated by higher valance Zr^{4+} ions. The decrease in grain size of codoped samples might be interpreted in terms of suppression of oxygen vacancies concentration, which slows oxygen ion motion and consequently grain growth [18].

According to the group theory, BFO with rhombohedral structure of $R3c$ space group has 18 optical phonon modes represented by $4A_1+5A_2+9E$. The A_1 and E modes are Raman and IR active, while A_2 modes remain Raman and IR inactive. Thus, for rhombohedral structure with $R3c$ space group, Raman active modes can be represented by 13 modes ($4A_1+9E$). Since Raman spectra is sensitive to the displacements of the atoms in the lattice, so it can provide significant information about lattice properties, ionic substitution, electric polarization, structural phase transitions and spin-phonon coupling. The substitution of smaller ionic radius and lighter mass Dy^{3+} ions at Bi-site induced a change in the stereochemical activity of Bi $6s^2$ lone pair by replacing Bi-O bond via Dy-O bond, which may affect electric polarization of BFO. In addition, the doping of larger ionic radius and

Download English Version:

<https://daneshyari.com/en/article/5438619>

Download Persian Version:

<https://daneshyari.com/article/5438619>

[Daneshyari.com](https://daneshyari.com)